

A Generalized Depth-Integrated Model of the Oceanic Mixed Layer

P. RAVINDRAN

Department of Oceanography, Dalhousie University, Halifax, Nova Scotia, Canada, and Biological Oceanography Section, Ocean Science Division, Department of Fisheries and Oceans, Bedford Institute of Oceanography, Dartmouth, Nova Scotia, Canada

DANIEL G. WRIGHT

Ocean Circulation Section, Ocean Science Division, Department of Fisheries and Oceans, Bedford Institute of Oceanography, Dartmouth, Nova Scotia, Canada

TREVOR PLATT

Biological Oceanography Section, Ocean Science Division, Department of Fisheries and Oceans, Bedford Institute of Oceanography, Dartmouth, Nova Scotia, Canada

SHUBHA SATHYENDRANATH

Department of Oceanography, Dalhousie University, Halifax, Nova Scotia, Canada, and Biological Oceanography Section, Ocean Science Division, Department of Fisheries and Oceans, Bedford Institute of Oceanography, Dartmouth, Nova Scotia, Canada

(Manuscript received 8 May 1996, in final form 2 June 1998)

ABSTRACT

A generalized depth-integrated model of the oceanic mixed layer is developed by considering the heat and energy budgets of the upper ocean. Unlike the Kraus–Turner-type bulk models, the assumptions of an a priori well mixed layer and a positive density discontinuity at the base of the layer are not required in the present formulation. Relaxation of these restrictions is achieved by dealing directly with time-integrated equations, thus eliminating inaccuracies introduced by forming a differential equation prior to time discretization. The formulation involves a careful accounting of the effects of stratification below the mixed layer and the change in the density of the mixed layer produced by heat absorption and freshwater exchange. Scale analysis of the equation governing changes in mixed layer depth is used to reveal the conditions under which the present model reduces to a standard Kraus–Turner-type bulk model. Model results are compared with observations at OWS Papa in order to confirm the utility of the formulation in a simple one-dimensional application. Potential use of this model for embedding mixed layer thermodynamics into large-scale circulation models is addressed.

1. Introduction

Physical and biogeochemical processes in the surface mixed layer of the ocean are sensitive to the seasonal evolution of the layer depth and temperature. By regulating the transfer of mass and energy across the sea surface, the mixed layer influences various atmospheric processes. By acting as a buffer between the deep ocean

and the atmosphere, it also regulates the global biogeochemical cycle. Understanding of the processes responsible for the formation and the evolution of the mixed layer provides an essential background to studies of upper-ocean dynamics, air–sea interaction, and biogeochemical cycles.

To this end, numerous attempts have been made to model the surface layer of the ocean. In general, such models can be classified into two groups: differential models and depth-integrated bulk models. Many of the commonly used, differential models share the theoretical foundation introduced by Mellor and Yamada (1974). These models have proven extremely useful in studies of the surface and bottom boundary layers. One

Corresponding author address: Dr. P. Ravindran, Faculty of Computer Science, DalTech, Dalhousie University, 1632-Maritime Center, Halifax NS B3J 2X4, Canada.
E-mail: indran@cs.dal.ca

of the characteristics of these models, which restricts their wider usage, is their substantial computational requirement (Martin 1986). Bulk models (such as Denman 1973; Niiler and Kraus 1977; Garwood 1977; and Gaspar 1988) share a common origin in Kraus and Turner (1967). These models are developed by integrating the heat and energy conservation equations over the mixed layer and are computationally more efficient than differential models. However, the simplicity and computational advantage of bulk models may be overshadowed by assumptions (often implicit) used in model formulations. Two notable assumptions are (i) a well mixed layer exists a priori and (ii) there is a density discontinuity at the base of the mixed layer.

As a contribution to the continuing development of efficient and more generally applicable mixed layer models, we present here a generalized depth-integrated model (GDIM) of the upper ocean. This model provides a general, but conceptually simple, description of the physical processes associated with the development of the oceanic mixed layer, within the framework of the bulk approach to mixed layer modeling.

To determine the evolution of the mixed layer depth, the change in potential energy of the upper ocean due to buoyancy inputs is balanced against the kinetic energy input. The heat budget of the upper ocean is used to determine the mixed layer temperature. This basic approach has been used previously in oceanography (Turner 1969; Simpson et al. 1978), but its potential for formulating a bulk mixed layer model has not been exploited.

The general features of the model ocean and the basic theory are presented in section 2. Mathematical expressions for the energetics of various physical processes considered in the model formulation are derived in section 3. An equation describing the deepening of the mixed layer is derived in section 4 and a similar expression describing the depth of a shallowing mixed layer is derived in section 5. The temperature of deepening and shallowing mixed layers are considered in sections 6 and 7, respectively. A comparison between the GDIM and Kraus–Turner-type models is presented in section 8. The ability of the model to simulate the observed evolution of mixed layer depth and temperature at station Papa is examined in section 9. A general discussion of model features is presented in section 10.

2. The model ocean

The basic features of the model ocean are shown in Fig. 1. At the beginning of each discrete time step, the surface layer is characterized by a uniform density ρ_m , temperature T_m , and depth h_m . The time step Δt is chosen to be sufficiently small that, during the interval, the rates of the energy inputs to the ocean can be considered to remain constant. The absorption of solar radiation within the water column and the exchanges of heat and

freshwater at the sea surface alter the stratification of the layer. This may either stabilize or destabilize the water column. The turbulent kinetic energy (TKE) input to the water column always works to reduce the stratification. The erosion of stratification by TKE, and any mixing due to destabilizing buoyancy fluxes, are considered to occur instantaneously at the end of each discrete time step. If the buoyancy inputs destabilize the water column or if the TKE input during the time step exceeds that required to remove the stratification caused by buoyancy inputs, the surface layer will deepen through entrainment. On the other hand, if the TKE input is not sufficient to remove any new stratification in the surface layer, the layer will retreat to a shallower depth within which the TKE input is exactly sufficient for complete mixing.

During deepening of the mixed layer, water is entrained into the layer from below. To account for this, we specify an entrainment layer of thickness h_e (of initially unknown magnitude), defined as that portion of the thermocline through which the mixed layer will extend at the end of the time step. Then, we seek an expression for h_e as a function of the density distribution in the ocean at the beginning of the time step and the energy inputs across the sea surface during the time step. During the shallowing of the mixed layer, there is no entrainment; our aim in this case is to calculate the new mixed layer depth as that of the equilibrium layer within which the depth-integrated TKE input by the action of wind balances the stratification tendency produced by heat and freshwater inputs.

The total heat input $H(0)$ across the sea surface is divided into a penetrative component $I(0)$ and a nonpenetrative component $Q(0)$. The penetrative component represents about 50% of the incoming solar radiation. The nonpenetrative component represents the remaining portion of the solar radiation $\hat{I}(0)$, the fluxes of sensible heat $S(0)$ and latent heat $E(0)$, and the net long-wave radiation at the sea surface $L(0)$. Thus,

$$Q(0) = \hat{I}(0) + S(0) + E(0) + L(0). \quad (1)$$

All surface fluxes are defined to be positive when directed into the ocean.

The density is assumed to be a function of temperature and salinity. The density distribution in the (generally thin) entrainment layer $\rho_e(z)$ is assumed to be a linear function of depth z of the form

$$\rho_e(z) = \rho_b + a(z - h_m), \quad (2)$$

where ρ_b is the density and a is the density gradient immediately below the mixed layer. Nonlinear forms of $\rho_e(z)$ could easily be considered, but both clarity and generality are achieved by the simple form given here.

If the rate of input of TKE to the layer exceeds the rate of change of potential energy arising from stratification of the layer, the excess energy will be used to entrain water across the base of the mixed layer, resulting in deepening of the layer. The mixed layer

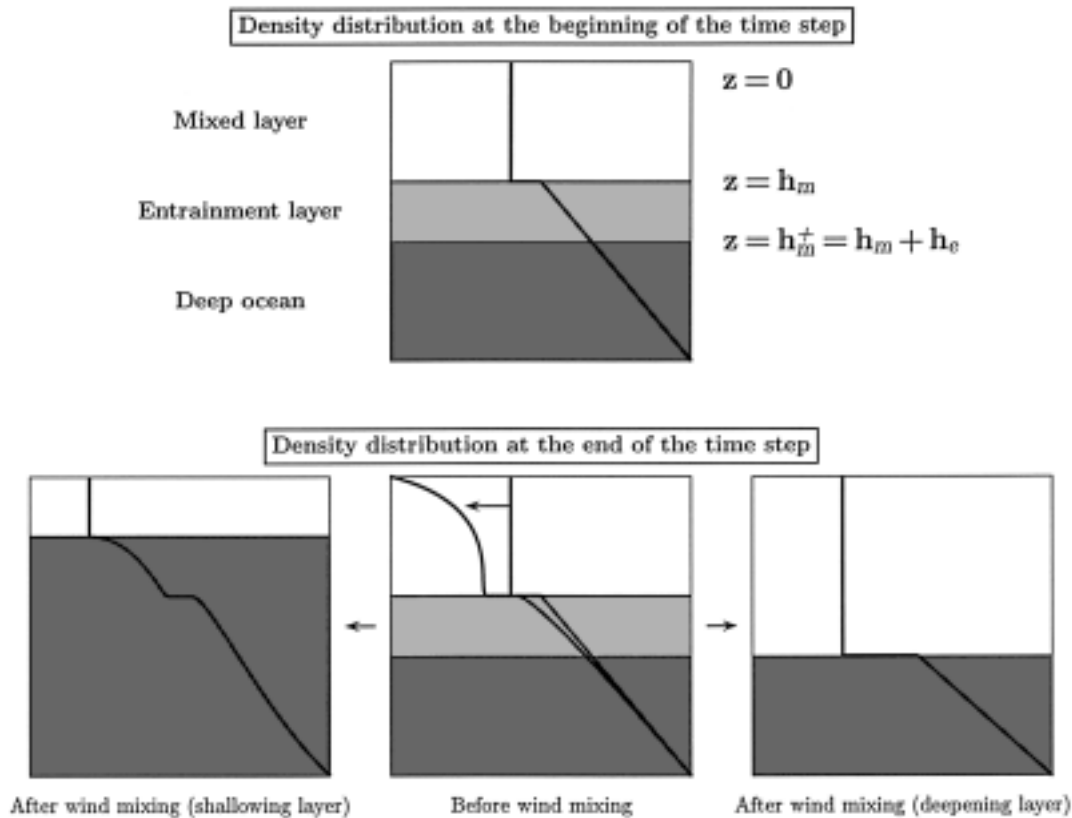


FIG. 1. The model ocean. The upper panel shows the conditions at the beginning of a time step, characterized by a surface layer overlying an entrainment layer. The lower middle panel shows the conditions at the end of the time step, where the density distributions in the mixed layer and the entrainment layer have been modified by the absorption of heat. The panels on the left and the right show two possible paths [deepening, given by Eq. (25) and shallowing, given by Eq. (27)] of mixed layer evolution depending upon the balance between the TKE input and the change in the potential energy associated with vertical mixing.

depth at the end of the time step is calculated by equating the change in the depth-integrated potential energy due to vertical mixing to the TKE input during the same time interval (cf. Turner 1969; Denman 1972; Simpson et al. 1978). Once the new mixed layer depth is known, the corresponding layer temperature is determined by considering the heat budget of the layer.

The change in the potential energy (ϕ) resulting from vertical mixing of a layer of arbitrary thickness $z_2 - z_1$ can be written as

$$\phi(z_1, z_2) = \int_{z=z_1}^{z_2} [\rho(z) - \bar{\rho}]gz \, dz, \quad (3)$$

where $\bar{\rho}$ is the mean density of the layer, given by

$$\bar{\rho} = \left(\frac{1}{z_2 - z_1} \right) \int_{z=z_1}^{z_2} \rho(z) \, dz, \quad (4)$$

and $\rho(z)$ is the density of water at depth z before mixing.

Let $h_m^+ = h_m + h_e$ be the depth of the mixed layer at the end of the time step, during the deepening phase of

the layer evolution. In the model that is now to be developed, the total change in the potential energy $\phi(0, h_m^+)$ associated with mixing at the end of the time interval Δt is decomposed into three parts:

- 1) The change in the potential energy associated with the internal mixing within the surface layer [$\phi(0, h_m)$]. This accounts for the TKE required to remove the stratification developed in the surface layer during the time step.
- 2) The change in the potential energy associated with internal mixing of the entrainment layer, resulting in the removal of the stratification associated with the linear density distribution and the additional stratification caused by the absorption of solar radiation beneath the mixed layer [$\phi(h_m, h_m^+)$].
- 3) The change in potential energy associated with complete mixing between the surface layer and the entrainment layer, each of which is internally well mixed through processes described in (1) and (2) [$\bar{\phi}(0, h_m^+)$].

The total change in potential energy of a deepening mixed layer $\phi(0, h_m^+)$ can be expressed as

$$\phi(0, h_m^+) = \phi(0, h_m) + \phi(h_m, h_m^+) + \tilde{\phi}(0, h_m^+), \quad (5)$$

which follows from the identity

$$\begin{aligned} & \int_0^{h_m^+} [\rho(z) - \bar{\rho}]gz \, dz \\ &= \int_0^{h_m} [\rho(z) - \bar{\rho}^m]gz \, dz + \int_{h_m}^{h_m^+} [\rho(z) - \bar{\rho}^e]gz \, dz \\ &+ \int_0^{h_m^+} [\tilde{\rho}(z) - \bar{\rho}]gz \, dz. \end{aligned} \quad (6)$$

In Eq. (6), $\bar{\rho}^m$ and $\bar{\rho}^e$ are respectively the mean density of the initial mixed layer and the entrainment layer after internal mixing within these layers. Also, in Eq. (6),

$$\tilde{\rho}(z) = \bar{\rho}^m \quad \text{for } 0 \leq z \leq h_m$$

and

$$\tilde{\rho}(z) = \bar{\rho}^e \quad \text{for } h_m \leq z \leq h_m^+. \quad (7)$$

See Fig. 2 for a pictorial representation of the mixing processes described above.

In the following section, analytical expressions for each of these components are derived, which are then used to develop the equations describing the changes in depth and temperature of the layer during the time step Δt .

3. Changes in potential energy associated with mixing

a. Potential energy change due to mixing within the surface layer

Applying Eq. (3) to the surface layer, the change in the potential energy associated with vertical mixing in the layer can be expressed as

$$\phi(0, h_m) = \int_0^{h_m} [\rho(z) - \bar{\rho}^m]gz \, dz, \quad (8)$$

where $\rho(z)$ is the density profile in the surface layer, before mixing at the end of the time step, given by

$$\begin{aligned} \rho(z) &= \rho_m - \Delta t \left[\frac{\alpha}{C_p} \frac{-dI(z)}{dz} + \delta(z)F(0) \right] \\ &\text{for } 0 \leq z \leq h_m, \end{aligned} \quad (9)$$

where α is the coefficient of thermal expansion, C_p is the specific heat of seawater at constant pressure, and $\delta(z)$ is the Dirac-delta function, with properties $\delta(z) = 0$ for $z > 0$ and $\int_0^z \delta(z') \, dz' = 1$. In Eq. (9), $I(z)$ is the solar radiation reaching depth z and $F(0)$ is a measure of the surface buoyancy flux associated with freshwater

and nonpenetrative heat input at the sea surface, given by (see Bowden 1983)

$$F(0) = \frac{\alpha}{C_p} Q(0) + \rho_0 \beta s f, \quad (10)$$

where β is the coefficient of haline contraction of seawater, s is the salinity of the surface layer, and f is the net freshwater flux (precipitation minus evaporation) across the sea surface.

The depth average of Eq. (9) for $0 \leq z \leq h_m$ is

$$\bar{\rho}^m = \rho_m - \frac{\Delta t}{h_m} \left[\frac{\alpha}{C_p} [I(0) - I(h_m)] + F(0) \right]. \quad (11)$$

Substituting Eqs. (9) and (11) into Eq. (8) and performing the integration gives

$$\phi(0, h_m) = \Delta t \frac{g h_m}{2} \left[\frac{\alpha}{C_p} I(0) f_{h_m} + F(0) \right], \quad (12)$$

where

$$f_{h_m} = \frac{2}{I(0)} \left[\frac{I(0) - I(h_m)}{2} - \frac{1}{h_m} \int_0^{h_m} I(z) \, dz \right], \quad (13)$$

is a function that accounts for the depth distribution of heat input to the mixed layer by the penetrative component of solar radiation. The numerical value of the function f_{h_m} varies between 0 and 1; $f_{h_m} = 1$ when all the radiation is absorbed at the sea surface.

b. Potential energy change due to mixing within the entrainment layer

Applying Eq. (3) to the entrainment layer gives

$$\phi(h_m, h_m^+) = \int_{h_m}^{h_m^+} [\rho(z) - \bar{\rho}^e]gz \, dz, \quad (14)$$

where $\rho(z)$ is now the density profile in the entrainment layer before mixing at the end of the time interval Δt :

$$\begin{aligned} \rho(z) &= \rho_b + a(z - h_m) + \Delta t \frac{\alpha}{C_p} \frac{dI(z)}{dz} \\ &\text{for } h_m \leq z \leq h_m^+, \end{aligned} \quad (15)$$

and $\bar{\rho}^e$ is now the depth-averaged density of the entrainment layer, which, using Eq. (15), can be written as

$$\begin{aligned} \bar{\rho}^e &= \frac{1}{h_e} \int_{h_m}^{h_m^+} \rho(z) \, dz \\ &= \rho_b + \frac{a h_e}{2} - \frac{\Delta t}{h_e} \frac{\alpha}{C_p} [I(h_m) - I(h_m^+)]. \end{aligned} \quad (16)$$

Substituting Eqs. (15) and (16) into Eq. (14) and simplifying gives

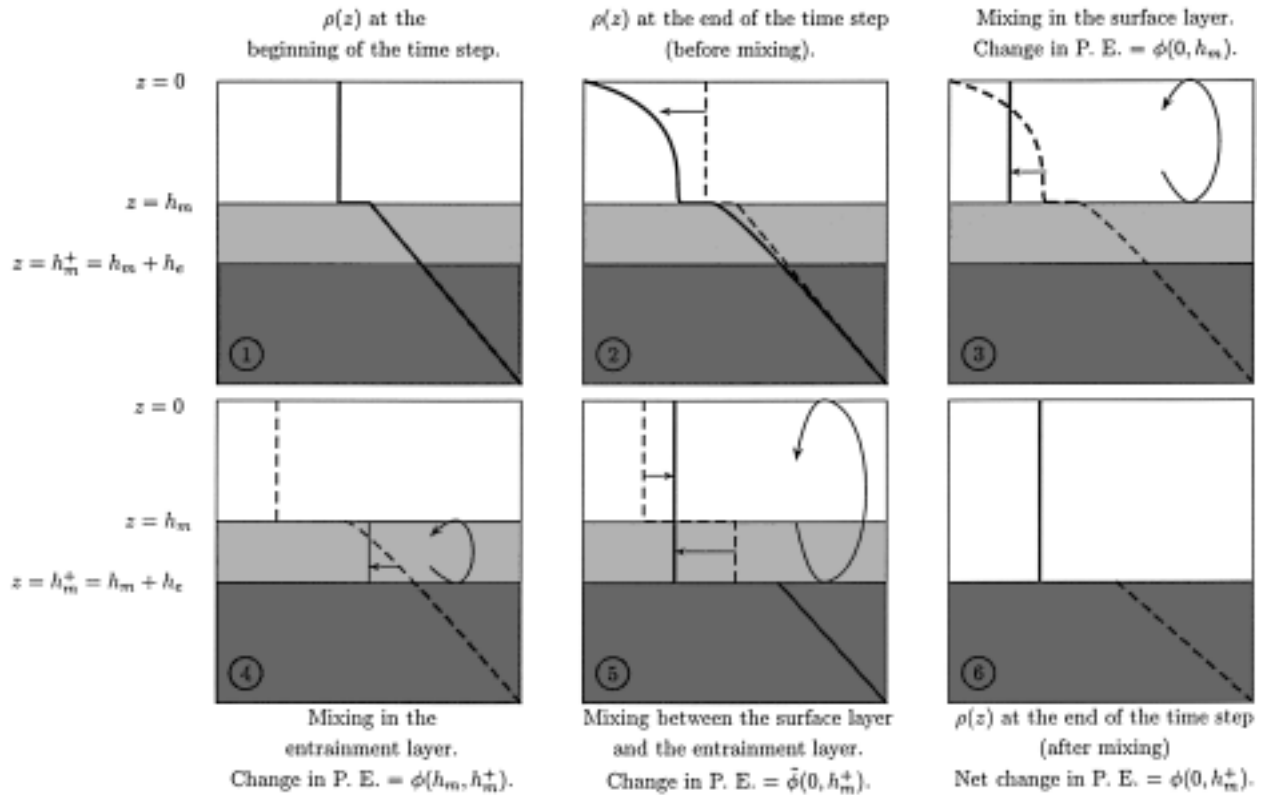


FIG. 2. Changes in the potential energy of the water column associated with wind mixing considered by the GDIM. The density distribution at the beginning of the time step is shown in panel 1. The modification to the density distribution at the end of the time step (before vertical mixing) resulting from the absorption of heat is shown in panel 2. Changes in the density distribution in the surface layer and in the entrainment layer resulting from internal mixing of the layers are shown in panels 3 and 4, respectively. The contributions from these processes to the total change in the potential energy of the water column are denoted by $\phi(0, h_m)$ and $\phi(h_m, h_m^+)$, respectively. The effect of mixing between the surface layer and the entrainment layer on the density distribution is shown in panel 5. The corresponding change in the potential energy is denoted by $\tilde{\phi}(0, h_m)$. The density distribution in the newly formed mixed layer is shown in panel 6. The total change in the potential energy associated with the formation of the new mixed layer is denoted by $\phi(0, h_m^+)$, which is given by $\phi(0, h_m^+) = \phi(0, h_m) + \phi(h_m, h_m^+) + \tilde{\phi}(0, h_m)$. The straight arrows indicate the change in the density distribution, and the curved arrows indicate the vertical extent of mixing considered in each panel.

$$\phi(h_m, h_m^+) = \frac{ag h_e^3}{12} + \Delta t \frac{g h_e}{2} \frac{\alpha}{C_p} I(h_m) f_{h_e}, \quad (17)$$

where

$$f_{h_e} = \frac{2}{I(h_m)} \left[\frac{I(h_m) + I(h_m^+)}{2} - \int_{h_m}^{h_m^+} I(z) dz \right]. \quad (18)$$

Equation (17) represents the change in the potential energy associated with the removal of stratification within the entrainment layer. The first term on the right denotes the contribution from the preexisting linear density gradient, and the second term represents that from the additional stratification produced by the absorption of solar radiation.

c. Potential energy change due to mixing between the initial mixed layer and the entrainment layer

The mixing between the surface layer and the entrainment layer is considered next, assuming that each

of these layers is already internally well mixed. From Eq. (3), the change in potential energy associated with the removal of the density difference between these layers can be expressed as

$$\tilde{\phi}(0, h_m) = \int_0^{h_m^+} [\tilde{\rho}(z) - \bar{\rho}] g z dz, \quad (19)$$

where $\tilde{\rho}(z)$ is the density profile after the internal mixing of the surface and entrainment layers. In the surface layer, $\tilde{\rho}(z) = \bar{\rho}^m$, as given by Eq. (11), and in the entrainment layer $\tilde{\rho}(z) = \bar{\rho}^e$, as given by Eq. (16).

The depth-averaged density of the mixed layer and the entrainment layer together, $\bar{\rho}$, can be written as

$$\bar{\rho} = \frac{1}{h_m^+} \int_0^{h_m^+} \tilde{\rho}(z) dz = \frac{1}{h_m^+} [\bar{\rho}^m h_m + \bar{\rho}^e h_e]. \quad (20)$$

Substituting Eq. (20) into Eq. (19) and simplifying gives

$$\tilde{\phi}(0, h_m^+) = \frac{gh_m h_e}{2} [\bar{\rho}^e - \bar{\rho}^m]. \quad (21)$$

d. Total change in potential energy for a deepening mixed layer

From Eqs. (5), (12), (17), and (21), the depth-integrated change in potential energy of a deepening mixed layer can be expressed as

$$\begin{aligned} \phi(0, h_m^+) = & \Delta t \frac{gh_m}{2} \left[\frac{\alpha}{C_p} I(0) f_{h_m} + F(0) \right] \\ & + \Delta t \frac{gh_e}{2} \frac{\alpha}{C_p} I(h_m) f_{h_e} + \frac{agh_e^3}{12} \\ & + \frac{gh_m h_e}{2} [\bar{\rho}^e - \bar{\rho}^m]. \end{aligned} \quad (22)$$

Substituting the expressions for $\bar{\rho}^m$ and $\bar{\rho}^e$ from Eqs. (11) and (16) into Eq. (22), we get

$$\begin{aligned} \phi(0, h_m^+) = & \Delta t \frac{gh_m}{2} \left[\frac{\alpha}{C_p} I(0) f_{h_m} + F(0) \right] + \frac{agh_e^3}{12} + \Delta t \frac{gh_e}{2} \frac{\alpha}{C_p} I(h_m) f_{h_e} \\ & + \frac{gh_m h_e}{2} \left\{ \rho_b - \rho_m + \frac{ah_e}{2} + \frac{\Delta t}{h_m} \left[\frac{\alpha}{C_p} [I(0) - I(h_m)] + F(0) \right] - \frac{\Delta t}{h_e} \frac{\alpha}{C_p} [I(h_m) - I(h_m^+)] \right\}, \end{aligned} \quad (23)$$

which is the total change in potential energy associated with the buoyancy redistribution through vertical mixing for a deepening mixed layer.

4. Depth of a deepening mixed layer

The change in potential energy associated with the formation of a new mixed layer through entrainment is determined by the equation

$$\Delta t(G - D) - \phi(0, h_m^+) = 0, \quad (24)$$

where G and D represent, respectively, the rates of generation and dissipation of TKE in the water column between 0 and h_m^+ . Substituting for $\phi(0, h_m^+)$ from Eq. (23) into Eq. (24) we have an expression for h_e , the increase in the depth of the mixed layer after time Δt :

$$\Delta t(G - D) - \Delta t \frac{gh_m}{2} \left[\frac{\alpha}{C_p} I(0) f_{h_m} + F(0) \right] = \frac{gh_m h_e}{2} \Delta \rho, \quad (25)$$

where $\Delta \rho$ is the “effective density difference” at the base of the mixed layer, given by the equation

$$\Delta \rho = \underbrace{\rho_b - \rho_m}_1 + \underbrace{\frac{\Delta t}{h_m} \left[\frac{\alpha}{C_p} [I(0) - I(h_m)] + F(0) \right]}_2 - \underbrace{\frac{\Delta t}{h_e} \frac{\alpha}{C_p} [I(h_m) - I(h_m^+)]}_3 + \underbrace{\frac{ah_e}{2}}_4 + \underbrace{\frac{\Delta t}{h_m} \frac{\alpha}{C_p} I(h_m) f_{h_e}}_5 + \underbrace{\frac{ah_e^2}{6h_m}}_6. \quad (26)$$

Equation (25) describes the energy budget of the upper ocean associated with the evolution of the mixed layer, under the influence of solar heating, surface heat and water exchanges, wind (or other) forcing, and dissipation. The left side of the equation represents the excess TKE available in the surface layer after removing the stratification resulting from buoyancy input to the original mixed layer. The right side of the equation identifies the energy required to deepen the mixed layer through a distance h_e by working against an “effective density difference” $\Delta \rho$ at the base of the mixed layer. Terms 1–4 of Eq. (26) give the actual density difference at the base of the mixed layer after

internal mixing within the separate surface and entrainment layers. The contributions are the density difference at the base of the mixed layer at the beginning of the time step (term 1), the changes in the density difference resulting from heat inputs to the mixed layer (term 2) and the entrainment layer (term 3), and the increase in the density difference at the base of the mixed layer resulting from the removal of the linear gradient in the density distribution in the entrainment layer (term 4). The last two terms of Eq. (26) are not actually contributions to the density difference at the base of the mixed layer. They account for the energy required to eliminate the stratifi-

cation within the entrainment layer [see Eq. (17)], resulting from the absorption of solar radiation (term 5) and the linear gradient in density (term 6), respectively. It is convenient to express these quantities in terms of an equivalent density difference at the base of the mixed layer, but their distinction from terms 1–4, accounting for the actual density difference at the base of the mixed layer, should be noted.

5. The depth of a shallowing mixed layer

When the TKE input to the mixed layer is not sufficient to counter the stratification produced by the input of heat and/or freshwater, the surface layer will retreat to a shallower level within which the TKE balances the buoyancy input. In such instances, entrainment cannot occur and the depth of the newly formed layer (h_m^+) is less than or equal to h_m . None of the terms in Eq. (25) that are functions of h_e contribute to the change in depth of the surface layer. Also, in Eq. (25), h_m can be replaced by h_m^+ since the layer depth is determined by the energy balance within the newly formed layer of depth h_m^+ , which is inde-

pendent of the surface-layer depth h_m at the beginning of the time step. The resulting equation is

$$\frac{gh_m^+}{2} \left[\frac{\alpha}{C_p} I(0) f_{h_m^+} + F(0) \right] - (G - D) = 0, \quad (27)$$

where

$$f_{h_m^+} = \frac{2}{I(0)} \left[\frac{I(0) + I(h_m^+)}{2} - \int_0^{h_m^+} I(z) dz \right]. \quad (28)$$

Equation (27) is identical to the equation used in Kraus–Turner-type mixed layer models to describe the shallowing of a mixed layer.

6. The temperature of a deepening mixed layer

Once the new layer depth (h_m^+) is known, the temperature of the layer (T_m^+) can be calculated from the surface-layer temperature at the beginning of the time step, the effects of the absorption of solar radiation, exchange of heat across the sea surface, and the entrainment of water across the base of the mixed layer. That is,

$$T_m^+ = \frac{h_m}{h_m^+} T_m + \frac{\Delta t}{\rho_0 C_p h_m^+} [I(0) - I(h_m^+) + Q(0)] + \frac{h_e}{h_m^+} \left(T_b - \frac{bh_e}{2} \right), \quad (29)$$

where the first term on the right accounts for the heat content of the mixed layer at the beginning of the time step, the second term accounts for the heat input from the nonpenetrative heat flux and the absorption of solar radiation, and the last term gives the change in the layer

temperature associated with the water entrained across the base of the surface layer. In Eq. (29), and b denotes the linear gradient in temperature within the entrainment layer.

For convenience, we rewrite (29) as

$$T_m^+ = T_m + \frac{\Delta t}{\rho_0 C_p h_m^+} [I(0) - I(h_m^+) + Q(0)] - \frac{h_e}{h_m^+} \left(T_m - T_b + \frac{bh_e}{2} \right).$$

7. The temperature of a shallowing mixed layer

Given the depth of a shallowing mixed layer, the layer temperature T_m^+ is calculated as the sum of the surface-layer temperature at the beginning of the time step and the increase in temperature produced by the heat absorption in the new mixed layer:

$$T_m^+ = T_m + \frac{\Delta t}{\rho_0 C_p h_m^+} [I(0) - I(h_m^+) + Q(0)]. \quad (30)$$

8. Comparisons with Kraus–Turner–type models

Figure 3 shows the vertical mixing scheme employed by the Kraus–Turner model (hereafter referred to as the

KT formulation). This can be compared against the mixing scheme shown in Fig. 2 to explain how the GDIM differs from the KT formulation:

- 1) In the first panels, any initial stratification within the entrainment layer is accounted for in the GDIM but neglected in the KT formulation. It should be noted that a buoyancy jump at the base of the mixed layer is essential for the KT formulation as if there were no buoyancy jump then the entrainment layer would already be part of the mixed layer. We shall see later that the assumption of a buoyancy jump at the base of the mixed layer can cause problems under exceptional (but realizable) circumstances.

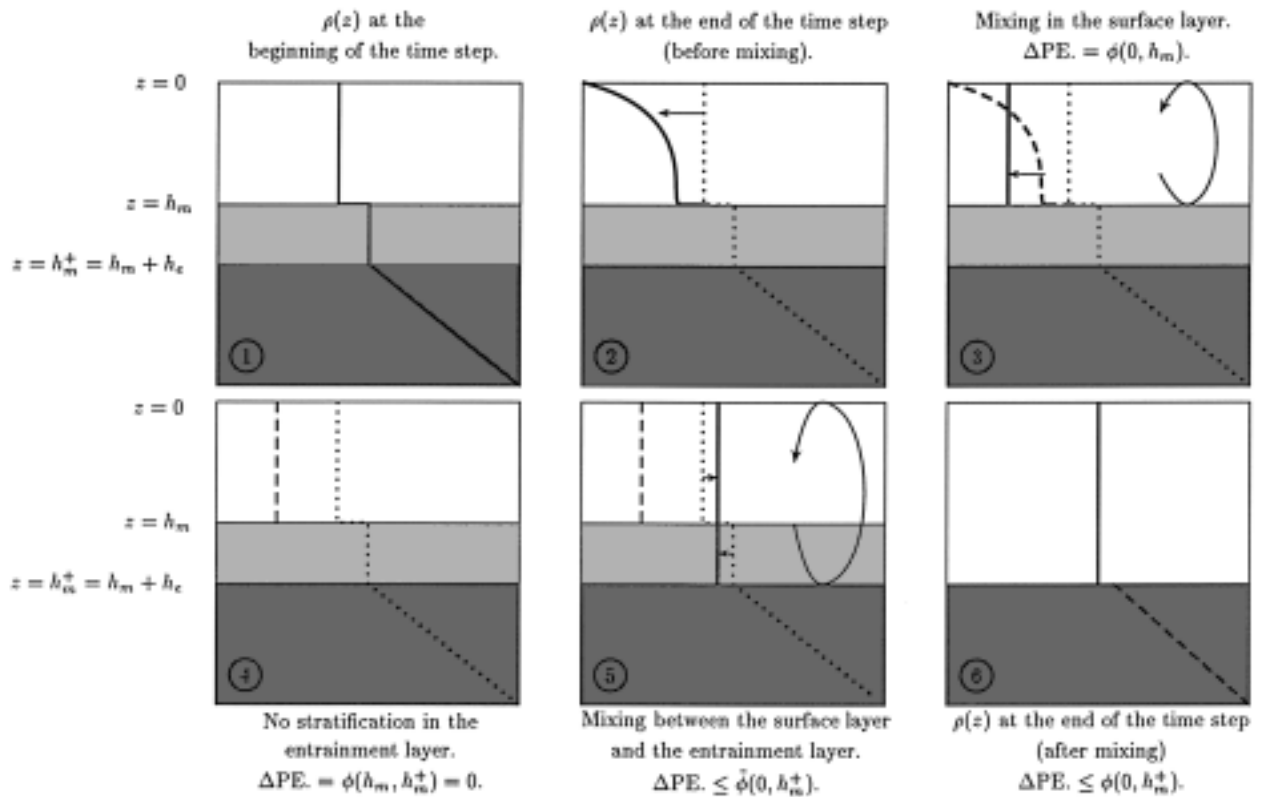


FIG. 3. A schematic representation of the vertical mixing scheme employed by the Kraus–Turner formulation. See section 8 of the text for a detailed description of the mixing process and a comparison with the GDIM mixing scheme illustrated in Fig. 2.

- 2) In the second panels we see that the absorption of solar radiation in the entrainment layer is accounted for in the GDIM but neglected in the KT formulation. This difference could become particularly important if the entrainment layer were to become more absorptive than the overlying mixed layer. In the extreme case, this could lead to static instability of the water column.
- 3) Another difference is associated with the treatment of buoyancy mixing within the surface layer (panel 3). In the KT formulation, the energy required to counter the stratification tendency in the surface layer is determined and subtracted from the energy available to drive entrainment, but the associated buoyancy change is not accounted for until the end of the mixing process (see panels 5 and 6). In the GDIM formulation, the change in buoyancy is accounted for at the time when the energy required for mixing is determined.
- 4) The fourth panel show that the energy required for vertical mixing within the entrainment layer is not taken into account in the KT formulation. This follows from the fact that the entrainment layer is taken to be initially well mixed, and the heat absorption in the layer is neglected. The energy required for mixing within the entrainment layer is specifically accounted for in the GDIM formulation.
- 5) As already mentioned in reference to the third panel, the KT formulation accounts for the energy required for vertical mixing within the surface layer, but the change in buoyancy of the surface layer is not accounted for until the end of the mixing process. Consequently, the energy required for mixing between the surface layer and the entrainment layer is determined based on the initial density distribution in the surface layer (dotted line), rather than the distribution after accounting for the buoyancy inputs during the current time step (dashed line). We anticipate that the effect of this approximation will only be significant when the preexisting density difference is very small.
- 6) The last panel show the density profile at the end of the time step, when the vertical mixing process is complete. Note that although the buoyancy change in the entrainment layer during the time step is not accounted by the KT formalism for estimating the energy required for entrainment, it is accounted for in determining the energy available to drive entrainment during the subsequent time step as modification to the density profile below the mixed layer.

It should be evident from the above comparison that the essential differences between the GDIM and the KT formulation are associated with estimating the density

jump at the base of the mixed layer and the stratification within the entrainment layer. These differences are further analyzed below.

If we assume that $h_e \propto \Delta t$ and consider the limiting case of Eq. (25) as $\Delta t \rightarrow 0$, we get

$$\frac{\partial h_m}{\partial t} = \lim_{\Delta t \rightarrow 0} \frac{h_e}{\Delta t} = \frac{2(G - D) - gh_m[(\alpha/C_p)I(0)f_{h_e} + F(0)]}{gh_m(\rho_b - \rho_m)}. \quad (31)$$

Equation (31) includes contributions only from the first term in (26) and is of the same form as the equation for $\partial h_m/\partial t$ used in KT-type models. Thus, the equation used to describe the deepening of a mixed layer by KT-type models represents a limiting case of Eq. (25). Further, it is clear that the differences are entirely due to the approximations used in the representation of the “effective density difference” at the base of the mixed layer.

Equation (31) is singular in the limits $h_m \rightarrow 0$ and $(\rho_b - \rho_m) \rightarrow 0$, and hence this equation cannot be used to determine changes in mixed layer depth in these limits. The flaw in the derivation of (31) is that the assumption $h_e \propto \Delta t$ is not valid in these limits. The more general equations (25) and (26) are valid in these limits.

In the absence of a surface mixed layer ($h_m = 0$), the entrainment layer will extend from the sea surface, and

therefore $I(h_m) = I(0)$. With this modification, Eq. (25) becomes

$$\Delta t(G - D) - \Delta t \frac{gh_e}{2} \left[\frac{\alpha}{C_p} I(0) f_{h_e} + F(0) \right] = \frac{agh_e^3}{12}. \quad (32)$$

This equation describes the development of a mixed layer in a linearly stratified water column in the presence of TKE input, absorption of solar radiation, and the exchange of heat across the sea surface. Note that the expression for h_e does tend to zero as $\Delta t \rightarrow 0$, but only as $(\Delta t)^{1/3}$, so the assumption $h_e \propto \Delta t$, leading to Eq. (31), is invalid. That is, when $h_m = 0$, the last term in Eq. (26) is $O(\Delta t)$ and must be retained even as $\Delta t \rightarrow 0$.

As $(\rho_b - \rho_m)$ decreases, each of the terms 2 through 6 in Eq. (26) increases in importance relative to term 1. In the limit $(\rho_b - \rho_m) \rightarrow 0$, at least one of these terms must be retained, reflecting the dependence on conditions below the mixed layer in this limit. Again $h_e \propto \Delta t$ is not valid for this limiting case.

The mixed layer depth predicted by Eqs. (25) and (31) will tend to the same value as the integration time step decreases, provided the condition $h_m(\rho_b - \rho_m) \neq 0$ is satisfied. However, with increasing time step, the mixed layer depth predicted by Eq. (31) will deviate from its true value. The discrepancy for any finite time step can be quantified by considering the nondimensional form of Eq. (26) obtained by dividing through by term 1:

$$\underbrace{\frac{\Delta \rho}{\rho_b - \rho_m} - 1}_i = \underbrace{\frac{\Delta t}{h_m} \left[\frac{\alpha}{C_p} [I(0) - I(h_m)] + F(0) \right]}_{ii} (\rho_b - \rho_m)^{-1} - \underbrace{\frac{\Delta t}{h_e} \frac{\alpha}{C_p} [I(h_m) - I(h_m^+)]}_{iii} (\rho_b - \rho_m)^{-1} + \underbrace{\frac{ah_e}{2}}_{iv} (\rho_b - \rho_m)^{-1} + \underbrace{\frac{\Delta t}{h_m} \frac{\alpha}{C_p} I(h_m) f_{h_e}}_v (\rho_b - \rho_m)^{-1} + \underbrace{\frac{ah_e^2}{6h_m}}_{vi} (\rho_b - \rho_m)^{-1}. \quad (33)$$

If we assume that terms (ii)–(vi) of Eq. (33) are negligible, then Eq. (25) reduces to Eq. (31), which is the general equation employed in KT formulation to describe the deepening of the mixed layer. However, neglecting terms (ii)–(vi) implies stringent conditions on the maximum time step that can be used in the model simulation. The conditions to be satisfied are

$$\Delta t \ll \frac{h_m(\rho_b - \rho_m)}{\left[\frac{\alpha}{C_p} [I(0) - I(h_m)] + F(0) \right]} \quad \text{from term (ii)} \quad (34)$$

$$\Delta t \ll \frac{h_e(\rho_b - \rho_m)}{\frac{\alpha}{C_p} [I(h_m) - I(h_m^+)]} \quad \text{from term (iii)} \quad (35)$$

$$\Delta t \ll \frac{h_m(\rho_b - \rho_m)}{\frac{\alpha}{C_p} I(h_m) f_{h_e}} \quad \text{from term (v)} \quad (36)$$

$$h_e \ll 2 \left(\frac{\rho_b - \rho_m}{a} \right) \quad \text{from term (iv)} \quad (37)$$

and

$$h_e \ll \sqrt{6h_m \left(\frac{\rho_b - \rho_m}{a} \right)} \quad \text{from term (vi)} \quad (38)$$

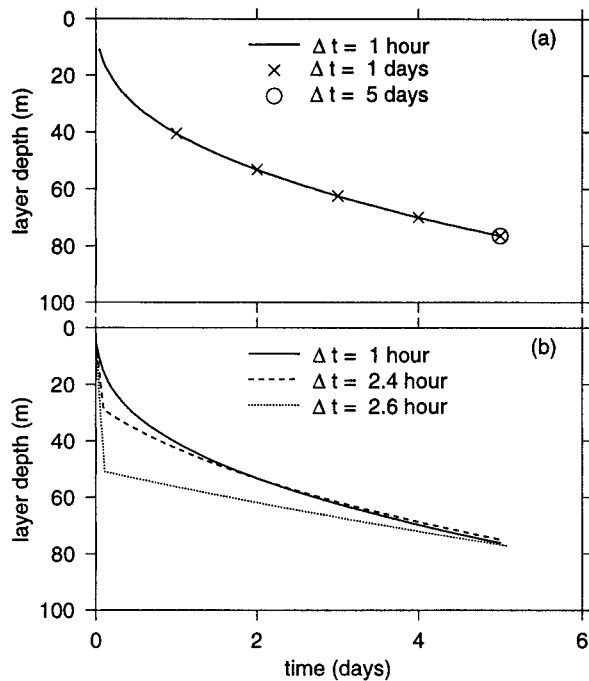


FIG. 4. The evolution of mixed layer depth under the influence of time-independent forcing during a 5-day period, simulated using Eq. (25), is shown in (a). The layer depth calculated using time steps of 1 day and 5 days are represented by “×” and circle, respectively. The results of model simulation using Eq. (31) are shown in (b). To ensure numerical stability of the integration routine, the maximum time step was limited to 2.6 h.

Note that, if $h_m(\rho_b - \rho_m) \neq 0$, then the last two conditions on h_e are equivalent to conditions on Δt because the increase in the layer depth during a time step is a function of the time step itself. Inequalities (34)–(38) limit the accuracy of KT formulation when the time step is chosen to be too large. If they are not satisfied, either the time step must be reduced, or the complete Eq. (25) must be used. We emphasize that the differential equation (31), obtained by taking the limit $\Delta t \rightarrow 0$, is an accurate representation of the physics of a deepening mixed layer if $h_m(\rho_b - \rho_m) \neq 0$. However, even in this case, the subsequent discretization using standard finite differences is less accurate than (25). Information regarding conditions beneath the mixed layer is lost in taking the limit $\Delta t \rightarrow 0$ and then returning to finite Δt based solely on the resulting differential equation.

One aspect of the computational efficiency afforded by Eq. (25) is illustrated in Fig. 4a, which shows several time series of mixed layer depth during a 5-day simulation of the model. The initial depth and temperature of the layer were 5 m and 24°C. The thermocline was characterized by a temperature gradient of 0.05°C m⁻¹ starting from a temperature of 23.5°C at the base of the mixed layer. The model ocean was forced with a wind stress of 0.4 Pa, a nonpenetrative heat flux of -400 W m⁻² and a penetrative solar radiation flux of 200 W m⁻². The net TKE input to the water column was specified as

$$(G - D) = \rho_0 m u_*^3, \quad (39)$$

where u_* is the friction velocity and $m = 0.65$ is the proportionality constant. From numerous parameterization schemes available for specifying the TKE input (see, e.g., Niiler and Kraus 1977), this particular form was selected for the sake of simplicity. Note that all forcing terms are constant in time.

The solid curve in Fig. 4a denotes the mixed layer depth calculated by Eq. (25) with a time step of 1 h. The corresponding values calculated using time steps of 1 day and 5 days are represented in the figure by “×” and circle, respectively. Mixed layer depths calculated using Eq. (31) with three different values of the time step are shown in Fig. 4b. To ensure numerical stability of the integration routine, the maximum time step was limited to 2.6 h. Figure 4a shows that the mixed layer depth predicted using Eq. (25) is not sensitive to the choice of time step, whereas Fig. 4b shows that the corresponding evolution based on Eq. (31) depends strongly on the time step, even for the case of constant forcing. The accuracy of the results presented in Fig. 4b is determined by the validity of the inequalities (34)–(38).

9. Comparisons with observations

To test mixed layer models reliably in the simplest possible context, data are required from a site for which a one-dimensional model in the vertical is applicable. Observations from OWS Papa (50°N, 150°W) provide an appropriate combination of weak advection, weak horizontal property gradients, and well-defined mixed layer variations. Oceanographic and meteorological observations from this site have been used in the past for testing and comparing the performances of mixed layer models (see, e.g., Martin 1985; Gaspar 1988; Large et al. 1994; Kantha and Clayson 1994).

Following previous investigators, we have tested the ability of the GDIM to simulate the seasonal progression of mixed layer depth and temperature at station Papa using 3-hourly observations for the year 1961. The heat flux components were calculated following the general procedure outlined in Martin (1985). The density of seawater was determined as a function of salinity and temperature, following Gill (1981). During the model simulation the temperature and salinity profile below the mixed layer were determined using vertical grids with 1-m resolution. The initial conditions and the ambient diffusivity below the mixed layer were specified according to Martin (1985).

The attenuation of solar radiation in the ocean was calculated according to Paulson and Simpson’s (1977) parameterization scheme. In the absence of field data to model the depth distribution of solar radiation in the water column, we have assumed that the optical characteristics of the water column can be represented by Type I of Jerlov (1976) classification scheme during the

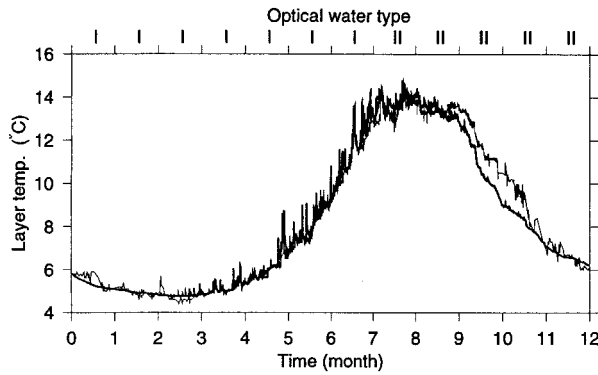


FIG. 5. A comparison between observed (thin curves) and the GDIM predicted (thick curves) time series of mixed layer temperature using 3-hourly observations of surface fluxes at station Papa during 1961.

first 7 months of the year and by Type II during the remainder. This assumption was made to get a best match between the observed and model-predicted layer temperature.

Gaspar's (1988) parameterization was used to estimate the net TKE input to the mixed layer. This is one of the most general schemes available for describing the TKE input within the framework of bulk mixed layer modeling. It explicitly takes into account the rotation- and stability-dependent changes in turbulent dissipation. The procedure followed for incorporating this parameterization into Eq. (25) is summarized in the appendix.

The observed and the GDIM predicted time series of mixed layer temperature are presented in Fig. 5, which shows an excellent match between the two for the first 9 months of the year. The discrepancy during the last 3 months may be due to the net input of heat by horizontal advection (Martin 1986). A comparison between the time series in Fig. 5 and the corresponding results from Martin (1985), Martin (1986), Large et al. (1994), and Kantha and Clayson (1994) suggests that the GDIM is very successful in reproducing the observed fields in comparison with many of the existing models.

Large et al. (1994) have suggested that an annual cycle of monthly mean difference between the model-predicted and observed temperature ($\overline{\Delta T_m}$) with values less than 0.5°C can be considered as a desirable model performance. Table I shows the values of $\overline{\Delta T_m}$ corresponding to Fig. 5. Except in the fall, $\overline{\Delta T_m}$ is less than 0.5°C . Table 6 of Large et al. (1994) shows corresponding values derived from model simulations at OWS Papa for the year 1961 using various bulk and differential models. A comparison between the two tables shows that the GDIM formulation gives smaller $\overline{\Delta T_m}$ values than many of the models presently used.

The time series of observed layer depth is given in Fig. 6a. It is derived from the temperature profiles by defining the base of the layer as the depth at which the temperature is 0.1°C less than the surface temperature. The GDIM predicted time series of mixed layer depth

TABLE 1. The difference between monthly mean values of the model-predicted and observed temperature. See Large et al. (1994) for a compilation of similar results from simulations of various bulk and differential models at OWS Papa.

Month	Temperature difference ($^\circ\text{C}$)
Jan	-0.06
Feb	-0.07
Mar	0.04
Apr	-0.11
May	0.04
Jun	-0.18
Jul	0.35
Aug	0.25
Sep	-0.10
Oct	-0.91
Nov	-0.63
Dec	-0.07

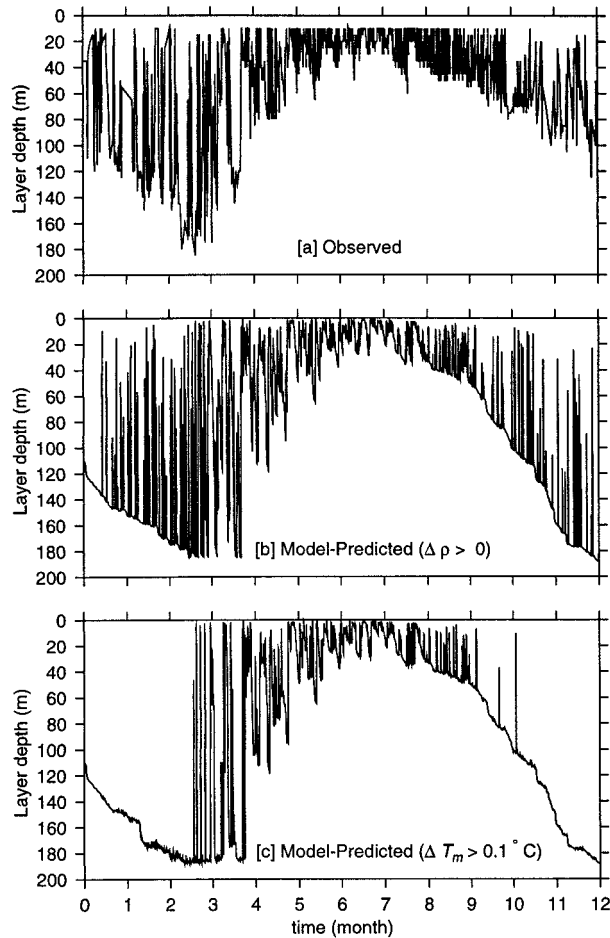


FIG. 6. A comparison between observed and model-predicted time series of mixed layer depth: (a) the layer depth derived from observed temperature profiles by assuming a temperature difference (ΔT_m) of 0.1°C at the base of the layer, (b) the layer depth predicted by the model, and (c) the layer depth derived from model-predicted temperature profiles following the same criterion of $\Delta T_m = 0.1^\circ\text{C}$ to define the base of the mixed layer.

is given in Fig. 6b. The layer depths derived from GDIM-predicted temperature profiles by following the same criterion used in Fig. 6a of assuming a 0.1°C temperature difference at the base of the mixed layer are shown in Fig. 6c. This somewhat arbitrary choice of the base clearly gives a deeper mixed layer in Fig. 6c than that given in Fig. 6b and filters out significant high-frequency oscillations in the mixed layer depth. However, this choice is required for direct comparison of our model results with observations shown in Fig. 6a and with previously reported model results.

A comparison between the time series of observed and the model-predicted mixed layer depths given in Fig. 6 shows that the GDIM is fairly successful in reproducing the observed evolution of mixed layer depth through summer. In the fall, the layer depth predicted by the GDIM is deeper than the observed, which is consistent with some of the results reported by Martin (1985), Martin (1986), Kantha and Clayson (1994), and Large et al. (1994). As in the case of layer temperature, this discrepancy may be caused by the horizontal advection of heat.

As the next step, we have compared the GDIM results against the results from a simulation using KT mixing formulation. The forcing fields and the initial conditions used for this simulation are identical to that used for the GDIM simulation. The KT formulation is derived from the GDIM by removing appropriate terms through the following steps.

- 1) The contributions from heat input to the mean density of the surface layer is neglected; that is, in Eq. (11), $\bar{\rho}^m = \rho_m$.
- 2) The mean density of the entrainment layer is taken to be the density at the base of the mixed layer; that is, in Eq. (16) $\bar{\rho}^e = \rho_b$.
- 3) The entrainment layer is assumed to be well mixed. Therefore, the energy required for vertical mixing in the entrainment layer is taken to be zero; that is, $\phi(h_m, h_m^+) = 0$.

The temperature predicted by the model is shown in Fig. 7a, along with the GDIM temperature distribution. Compared with the GDIM, the KT formulation simulates slightly deeper and cooler mixed layer. The difference between the layer temperature predicted by the two models is given in Fig. 7b as a percentage of the temperature predicted by the GDIM, which shows that the maximum difference in the layer temperature between the two models is about 4% of the temperature predicted by the GDIM. Most of the difference depicted in Fig. 7b can be attributed to the detailed accounting by the GDIM of the effect of heat input to the water column on the mean density of the mixed layer and the entrainment layer alone. This point is evident from the similarity between Figs. 7b and 7c in which we have plotted the difference in temperature predicted by GDIM and a Kraus–Turner approximation of the GDIM obtained by implementing only step 1 ($\bar{\rho}^m = \rho_m$) and step

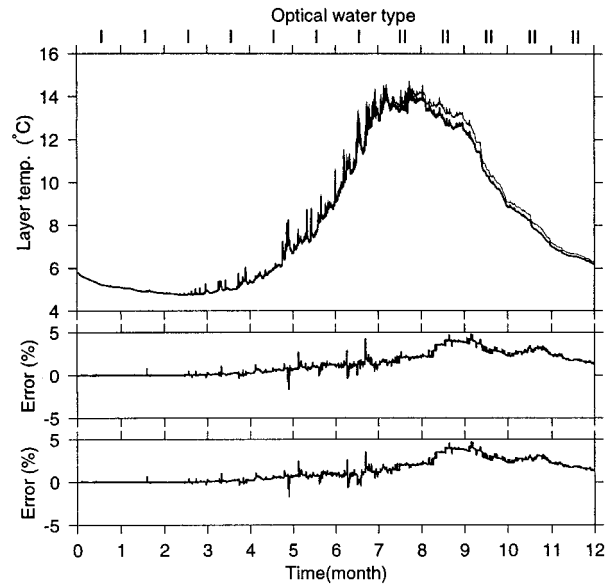


FIG. 7. Time series of mixed layer temperature predicted by the GDIM (thick curve) and the Kraus–Turner model derived from the GDIM (thin curve) are shown in (a). The relative error in the temperature predicted by the Kraus–Turner model is shown in (b) as percentage of the layer temperature predicted by the GDIM model, with a maximum relative error of about 4%. In (c) the relative error when the Kraus–Turner model is modified to account for the change in the potential energy of the entrainment layer. A comparison between (b) and (c) suggests that a significant portion of the difference between the results of the Kraus–Turner model and the GDIM is caused by the detailed accounting of the changes in the mean density of the mixed layer and the entrainment layer in the GDIM.

2 ($\bar{\rho}^e = \rho_b$), but accounting for the change in the potential energy of the entrainment layer [$\phi(h_m, h_m^+) \neq 0$].

10. Discussion

Bulk models of the oceanic mixed layer are conceptually simple and computationally efficient. They have also been successful in reproducing the observed fields of mixed layer depth and temperature (Martin 1985; Gaspar 1988). However, their wider applicability is limited by the requirements of the a priori existence of a well mixed layer and a positive density discontinuity at the base of the layer. The GDIM developed in this paper is free from these limitations. It yields improved accuracy and stability properties when finite time steps are used, as in all numerical implementations. Finally, the dynamical basis of the present model formulation has been made as transparent as possible in order to facilitate both understanding and future modifications.

An important difference between the GDIM and previous mixed layer models is the use of a time-integrated budget approach rather than a differential approach for the time dimension. Thus, in the GDIM, the bulk modeling approach has effectively been extended to include the time dimension as well as the vertical dimension. In this sense, the present formulation is further distin-

guished from the popular differential models (e.g., Mellor and Yamada 1974) and shifts further toward the energy budget model of Simpson et al. (1978).

As a consequence of using a time-integrated approach, several terms appear in Eq. (26) that do not appear in the standard KT formulation. If $h_m(\rho_b - \rho_m) \neq 0$, then each of these terms are $O(\Delta t)$ (i.e., they tend to zero at least as fast as Δt), so that they are correctly eliminated in the limit $\Delta t \rightarrow 0$, which is used in the differential approach. However, once eliminated, these terms are obviously not restored when the equations are expressed in discrete form, with finite Δt , as used in numerical integrations. If $h_m(\rho_b - \rho_m) = 0$, then Eq. (31) is not a valid limit of Eq. (25) even as $\Delta t \rightarrow 0$. The principal difference between the GDIM approach and those used in the past is that the validity of the new model is not restricted to the limit $\Delta t \rightarrow 0$.

Related to the improved accuracy for a given Δt is the numerical stability of the finite-difference formulation. As evident from Fig. 4b, the numerical procedure used to determine the evolution of mixed layer depth in the standard KT formulation is unstable if the time step is not chosen sufficiently small. As a consequence, during model simulations using observed data, the time step of integration is generally determined by the requirement for numerical stability rather than the frequency of observations or the timescales on which the forcing varies. On the other hand, the depth of the mixed layer predicted by the GDIM formulation is not sensitive to the size of the time step used, provided temporal variations in the forcing functions are resolved. Therefore, model simulations using the GDIM formulation can be optimized for computational efficiency by choosing the time interval between observations (or between significant changes in the observations) as the time step for model simulation.

It should be emphasized that the results in Fig. 4 depend critically on the specification of constant forcing. Accurate estimation of mixed layer evolution requires that temporal variations in the forcing fields be resolved. For example, a period of intense cooling or strong wind mixing followed by a mild condition will modify the thermal structure at greater depths than if the mean condition persisted throughout the same time interval. Nevertheless, large-scale models of oceanic circulation and air-sea interactions are often used in climatic research studies with time steps ranging from a few hours to a month. Incorporation of mixed layer dynamics in such models is clearly of interest. Unfortunately, the computational burden of such model is very large and it is highly desirable to minimize the additional requirements of any new model components. The effect of nonlinearity in the forcing fields on mixed layer evolution is an important factor to be considered while incorporating mixed layer models into such large-scale models. This is because a larger time step can lead to poor sampling of the forcing fields, which in turn, will lead to poor performance of the mixed layer model.

In such instances, the nonlinearity should be either resolved or parameterized. The choice depends on the balance between the desire for computational efficiency and accuracy. Better parameterization of the effects of nonlinearity will lead to improved efficiency. Attempts have been made in the past to achieve this goal (see, e.g., Woods and Barkman 1986). However, the numerical stability imposes a constraint on the size of the time step that can be used for integration of the KT formulation. This limits the applicability of the model to study the effect of nonlinear forcing, with timescales more than a few hours, on mixed layer evolution. This is because, when the KT formulation is integrated with larger time steps, it will be difficult to distinguish between the error caused by nonlinear forcing and the error caused by numerical instability. As evident from Fig. 4, the GDIM formulation is numerically more stable than the KT formulation and therefore better suited for such studies.

In general, the performance of the GDIM is on a par with any of the commonly used bulk or differential models. The primary advantages of the GDIM over previous bulk models lies in its increased computational efficiency associated with numerical stability and in the elimination of singularities associated with the conditions $h_m \rightarrow 0$ and $(\rho_b - \rho_m) \rightarrow 0$.

There have been several attempts to incorporate thermodynamic processes into models of the upper-ocean dynamics (Schopf and Cane 1983; McCreary and Kundu 1989; McCreary et al. 1993). A major difficulty in incorporating KT-type mixed layer models into dynamic models of the upper ocean is the requirement of a positive density discontinuity at the base of the mixed layer. In the presence of surface cooling or advective effects, the density discontinuity at the base of the layer may disappear ($\rho_b = \rho_m$), and this introduces a mathematical singularity in the equation used to describe the evolution of the mixed layer depth [Eq. (31)]. Attempts to overcome this difficulty have involved estimation of the effective temperature difference based on the temperature distribution in the thermocline (Schopf and Cane 1983). The GDIM provides a better solution to this problem as the information from beneath the mixed layer is naturally, and appropriately, used in the new model [see Eq. (26)].

Further improvements in our model performance are expected to come from improved representations of the TKE budget. Allowing for the effects of processes such as internal wave breaking and biologically driven optical variability are potentially important, even in one-dimensional models. In addition, the effects of horizontal and vertical advection by both Langmuir circulation and large-scale current fields must be included to handle more general cases (Large et al. 1994; Li and Garrett 1997).

A number of schemes with different degrees of complexity and different physical foundations are available for describing the TKE budget (Zilitinkevich et al. 1979; Garwood 1979; Gaspar 1988). Equation (25) is not restricted to any particular set of parameterizations for

representing the TKE input to the ocean, and it can be easily adapted to any scheme one may select. The simplicity and generality of Eq. (25) result in a useful framework for testing and intercomparison of various parameterizations of the TKE budget.

In regions such as the equatorial oceans, shear-induced mixing in the thermocline can play an important role in the deepening of the mixed layer. To account for this effect, Chen et al. (1994) have developed a hybrid mixing scheme in which the evolution of the mixed layer is described using the KT formulation, and the evolution of the thermocline is described using the vertical mixing scheme of Price et al. (1986), which is based on the critical Richardson number criterion. A better accounting of stratification below the base of the mixed layer could be included into this hybrid scheme by replacing the KT formulation by the GDM formulation. The more general applicability and improved representation of effects that enter at finite Δt , together with the additional computational efficiency resulting from the larger time steps that can be tolerated by the present formulation, make it well suited for incorporating mixed layer thermodynamics into three-dimensional circulation models of the upper ocean.

Acknowledgments. We thank Dr. Barry Ruddick and two anonymous reviewers for comments and suggestions that helped to improve the quality of the manuscript and Mr. Josko Bobanovic and Dr. Paul J. Martin for making available the dataset from OWS Papa. PR thanks Dr. George N. White III, Ms. H. Maass, and Ms. L. Payzant for valuable assistance during the course of this study. The work presented in this paper was supported, in part, by the Office of Naval Research (USA); National Aeronautics and Space Administration (USA) and the Department of Fisheries and Oceans, Canada. Additional support was provided by the Natural Sciences and Engineering Research Council (Canada) through grants to TP and SS. This work was carried out

as part of the Canadian contribution to the Joint Global Ocean Flux Study.

APPENDIX

The TKE Formulation and Numerical Implementation

Equation (25) can be written in the form

$$(G - D) - \frac{1}{2}\rho_0 h_m B(h_m) = \frac{g h_m h_e}{2\Delta t} \Delta\rho, \quad (\text{A1})$$

where

$$B(h_m) = \frac{g}{\rho_0} \left[\frac{\alpha}{C_p} I(0) f_{h_m} + F(0) \right]. \quad (\text{A2})$$

Following Gaspar (1988), the net TKE input to the mixed layer can be specified as

$$(G - D) = \rho_0 \left[(m_2 + m_3) u_*^3 - \frac{h_m}{l} E_m^{3/2} \right], \quad (\text{A3})$$

where $m_2 = 2.6$ and $m_3 = 1.9$ are transfer coefficients associated with the surface momentum flux and production of TKE from vertical shear within the mixed layer respectively, l is a dissipation-length scale, and E_m is twice the mean eddy kinetic energy integrated over the layer depth. Substituting Eq. (A3) into Eq. (A1) we get

$$(m_2 + m_3) u_*^3 - \frac{h_m}{l} E_m^{3/2} - \frac{1}{2} h_m B(h_m) = \frac{g h_m h_e}{2\Delta t \rho_0} \Delta\rho. \quad (\text{A4})$$

Noting the conversion $w_e = \Delta h/\Delta t$ and $\Delta b = g\Delta\rho/\rho_0$ we see that Eq. (A4) is identical to Eq. (35) of Gaspar (1988) except for the specification of $\Delta\rho$. In Eq. (A4), $\Delta\rho$ is determined using Eq. (26), whereas in Eq. (35) of Gaspar (1988) only the first term on the right of Eq. (26) is used to determine $\Delta\rho$.

Equation (50) of Gaspar (1988) gives the solution to Eq. (A4), which can be rearranged as

$$\frac{\Delta t \rho_0}{2} \left[\frac{-(0.5A_p + c_{pl}S_p) + [(0.5A_p - c_{pl}S_p)^2 + 2c_4(h_m/l)^2 A_p S_p]^{1/2}}{c_4(h_m/l)^2 - c_{pl}} \right] = \frac{g h_m h_e}{2} \Delta\rho. \quad (\text{A5})$$

Equation (A5) is the particular form of Eq. (25) using the Gaspar (1988) parameterization of the TKE budget, in which

$$A_p = c_{p3} u_*^3 - c_{pl} h_m B(h_m), \quad (\text{A6})$$

$$S_p = (m_2 + m_3) u_*^3 - \frac{1}{2} h_m B(h_m), \quad (\text{A7})$$

$$c_{pl} = [(2 - 2m_5)(l_p/l) + m_4]/6, \quad (\text{A8})$$

$$c_{p3} = [m_4(m_2 + m_3) - (l_p/l)(m_2 + m_3 - m_5 m_3)]/3, \quad (\text{A9})$$

and

$$c_4 = 2m_4/m_1^2. \quad (\text{A10})$$

In the above equations, l and l_p are dissipation length scales defined by the equations

$$\frac{h_m}{l} = a_1 + a_2 \max \left[1, \frac{h_m}{0.4\lambda} \right] e^{h_m/L} \quad (\text{A11})$$

and

$$\frac{h_m}{l_p} = a_1 + a_2 e^{h_m/L}, \quad (\text{A12})$$

where

$$L = \frac{u_*^3}{B(h_m)} \quad (\text{A13})$$

is the Monin–Obukhov length. Note that in Eqs. (A5) to (A12), $m_1 = 0.45$, $m_4 = 2.3$, $m_5 = 0.6$, $a_1 = 0.6$, and $a_2 = 0.3$ are parameters defined by Gaspar (1988).

During each time step, the new layer depth is initially calculated under the assumption that the mixed layer is in a shallowing phase by solving the equation $A_p = 0$. If the estimated layer depth is greater than the mixed layer depth at the beginning of the time step, the mixed layer is in a deepening phase. Therefore, the estimated value is discarded, and the depth of the mixed layer is estimated by solving Eq. (A5) together with Eq. (26).

Any combination of strong wind, surface cooling, and relatively small density discontinuity at the base of the mixed layer can cause rapid deepening of the mixed layer. Under such conditions, a single-step solution to Eq. (A5) can be inaccurate due to the assumption of a linear density gradient over several meters. This potential problem is controlled by solving Eq. (A5) through an iterative procedure as follows.

The excess TKE, ζ_0 , available within the initial mixed layer after removing the internal stratification is estimated from the right-hand side of Eq. (A5) as

$$\zeta_0 = (G - D) - \phi(0, h_m). \quad (\text{A14})$$

The TKE required for vertical mixing in an entrainment layer of 1-m thickness [$\phi(h_m, h_m + 1)$] and for mixing between the initial mixed layer and this entrainment layer [$\tilde{\phi}(0, h_m + 1)$] are calculated from Eqs. (17) and (21), respectively.

The excess energy ζ_1 available after deepening the mixed layer through 1 m is calculated as

$$\zeta_1 = \zeta_0 - \phi(h_m, h_m + 1) - \tilde{\phi}(0, h_m + 1). \quad (\text{A15})$$

If $\zeta_1 > 0$, the new layer depth is estimated as

$$h_m^1 = h_m + 1,$$

and the layer density is updated using Eq. (20).

The excess energy available after increasing the layer depth by another 1 m is calculated as

$$\zeta_2 = \zeta_1 - \phi(h_m^1, h_m^1 + 1) - \tilde{\phi}(0, h_m^1 + 1), \quad (\text{A16})$$

or, in general, for the i th round of iteration

$$\zeta_i = \zeta_{i-1} - \phi(h_m^{i-1}, h_m^{i-1} + 1) - \tilde{\phi}(0, h_m^{i-1} + 1). \quad (\text{A17})$$

If $\zeta_i > 0$, the depth of the mixed layer is again incre-

mented by 1 m, the mixed layer density is updated, and the procedure is repeated till a depth interval $\{(h_m + n - 1), (h_m + n)\}$ is determined within which ζ_i becomes negative. Once this interval is identified, the final layer depth h_m^+ in the range $h_m^{n-1} < h_m^+ < h_m^n$ can be estimated by continuing the iteration with smaller values of h_e or by using a standard bisection procedure.

The advantage of using this procedure is that during the i th round of iteration the assumption of a linear density gradient needs to be true only in the 1-m interval $\{(h_m + i - 1), (h_m + i)\}$.

REFERENCES

- Bowden, K. F., 1983: *Physical Oceanography of Coastal Waters*. Ellis Horwood Series in Marine Science, Halsted Press, 302 pp.
- Chen, D., R. Rothstein, and A. J. Busalacchi, 1994: A hybrid vertical mixing scheme and its application to tropical ocean models. *J. Phys. Oceanogr.*, **24**, 2156–2179.
- Denman, K. L., 1972: The response of the upper ocean to meteorological forcing. Ph.D. thesis, University of British Columbia, Vancouver, 118 pp.
- , 1973: A time-dependent model of the upper ocean. *J. Phys. Oceanogr.*, **3**, 173–184.
- Garwood, R. W., 1977: An oceanic mixed-layer model capable of simulating cyclic states. *J. Phys. Oceanogr.*, **7**, 455–468.
- , 1979: Air–sea interaction and dynamics of the surface mixed layer. *Rev. Geophys. Space Phys.*, **17**, 1507–1524.
- Gaspar, P., 1988: Modeling the seasonal cycle of the upper ocean. *J. Phys. Oceanogr.*, **18**, 161–180.
- Gill, A. E., 1981: *Atmosphere–Ocean Dynamics*. Academic Press, 662 pp.
- Jerlov, N. G., 1976: *Marine Optics*. Elsevier, 231 pp.
- Kantha, L. H., and C. A. Clayson, 1994: An improved mixed-layer model for geophysical application. *J. Geophys. Res.*, **99**, 25 235–25 266.
- Kraus, E. B., and J. S. Turner, 1967: A one-dimensional model of the seasonal thermocline. II. The general theory and its consequences. *Tellus*, **19**, 98–105.
- Large, W. G., J. C. McWilliams, and J. S. Turner, 1994: Oceanic vertical mixing: A review and a model with a nonlocal boundary layer parameterization. *Rev. Geophys.*, **32**, 363–403.
- Li, M., and C. Garrett, 1997: Mixed layer deepening due to Langmuir circulation. *J. Phys. Oceanogr.*, **27**, 121–132.
- Martin, P. J., 1985: Simulation of the mixed layer at OWS November and Papa with several models. *J. Geophys. Res.*, **90**, 903–916.
- , 1986: Testing and comparison of several mixed-layer models. NORDA Tech. Rep. 143, NSTL, Bay St. Louis, Mississippi, 30 pp.
- McCreary, J. P., and P. K. Kundu, 1989: A numerical investigation of sea surface temperature variability in the Arabian Sea. *J. Geophys. Res.*, **94**, 16 097–16 114.
- , —, and R. L. Molinari, 1993: A numerical investigation of dynamics, thermodynamics and mixed-layer processes in the Indian ocean. *Progress in Oceanography*, Vol. 31, Pergamon, 181–244.
- Mellor, G. L., and T. Yamada, 1974: A hierarchy of turbulent closure models for planetary boundary layers. *J. Atmos. Sci.*, **31**, 1791–1806.
- Niiler, P. P., 1975: Deepening of the wind-mixed layer. *J. Mar. Res.*, **33**, 405–422.
- , and E. B. Kraus, 1977: One-dimensional models of the upper ocean. *Modelling and Prediction of the Upper Layers of the Ocean*, E. B. Kraus, Ed., Pergamon, 143–172.
- Paulson, C. A., and J. J. Simpson, 1977: Irradiance measurements in the upper ocean. *J. Phys. Oceanogr.*, **7**, 952–956.
- Price, J. F., R. A. Weller, and R. Pinkel, 1986: Diurnal cycling: Ob-

- servations and models of upper ocean response to diurnal heating, cooling, and wind mixing. *J. Geophys. Res.*, **91**, 8411–8427.
- Schopf, P. S., and M. A. Cane, 1983: On equatorial dynamics, mixed-layer physics and sea surface temperature. *J. Phys. Oceanogr.*, **13**, 917–935.
- Simpson, J. H., C. M. Allen, and N. C. G. Morris, 1978: Fronts on the continental shelf. *J. Geophys. Res.*, **83** 4607–4614.
- Turner, J. S., 1969: A note on wind mixing at the seasonal thermocline. *Deep Sea Res.*, **16**, 297–300.
- Woods, J. D., and W. Barkmann, 1986: The response of the upper ocean to solar heating. I: The mixed layer. *Quart. J. Roy. Meteor. Soc.*, **112**, 1–27.
- Zilitinkevich, S. S., D. V. Chalikov, and Y. D. Resnyansky, 1979: Modelling the oceanic upper layer. *Oceanol. Acta*, **2**, 219–240.